Nonlinear Structure of the Diffusing Gas-Metal Interface in a Thermonuclear Plasma

Kim Molvig,[1,2] Erik L. Vold,[1] Evan S. Dodd,[1] and Scott C. Wilks[3]
[1]Los Alamos National Laboratory, Los Alamos, New Mexico 87545, USA
[2]Massachusetts Institute of Technology, Cambridge, Massachusetts 02139, USA
[3]Lawrence Livermore National Laboratory, Livermore, California, 94550, USA
(Received 28 May 2014; published 1 October 2014)

This Letter describes the theoretical structure of the plasma diffusion layer that develops from an initially sharp gas-metal interface. The layer dynamics under isothermal and isobaric conditions is considered so that only mass diffusion (mixing) processes can occur. The layer develops a distinctive structure with asymmetric and highly nonlinear features. On the gas side of the layer the diffusion coefficient goes nearly to zero, causing a sharp "front," or well defined boundary between mix layer and clean gas with similarities to the Marshak thermal waves. Similarity solutions for the nonlinear profiles are found and verified with full ion kinetic code simulations. A criterion for plasma diffusion to significantly affect burn is given.

DOI: 10.1103/PhysRevLett.113.145001 PACS numbers: 28.52.Cx, 47.45.-n, 52.40.Hf, 52.57.-z

Fusion yield degradation in inertial confinement fusion (ICF) capsule implosions has long been attributed to the mixing of pusher material into the fuel as a result of hydrodynamic instabilities, turbulence, and flow asymmetries that stir the fuel-pusher interface. The hydrodynamic stirring motions provide macroscopic interpenetration of the materials that are eventually mixed atomically by a microscopic diffusion process. The atomic mixing is necessary if fusion burn reduction is to result. And yet the models in use today [1,2] have no dependence on plasma diffusion. It is assumed that the rate limiting process is determined by the large-scale hydrodynamic cascade. Diffusion in the mixing process is analogous to viscosity in the Kolmogorov concept of eddy turbulence. The turbulent shear layer of neutral fluids provides a simplified paradigm for how the mix models of high density fusion are supposed to work. A model [3] for these shear layers computes the growth in time of the interfacial area, using scaling and similarity arguments that extend the homogeneous turbulence picture of Kolmogorov. The model [3] predicts that the interfacial area grows by a factor comparable to the ratio of the integral scale to the dissipation scale, or $L/\lambda_K \sim R_e^{3/4}$. At high R_e this is an enormous number. It means that an atomically mixed layer of width $\Delta x_L \sim L R_e^{-3/4}$ normal to the interfacial surface is sufficient to fill the entire stirred volume. The scaling arguments of Ref. [3] give the time for the interfacial area increase as comparable to the integral scale time $\tau_I \sim L/U$. But in the time τ_I diffusion produces a layer width $\Delta x_D \sim \sqrt{DL/U} \sim L R_e^{-1/2} \sim R_e^{1/4} \Delta x_L$ (taking the Schmidt number of order unity), or $\Delta x_D \gg \Delta x_L$. The enormous increase in interfacial area overwhelms diffusion as the rate limiting factor in the overall process.

Diffusion is fundamental to the production of a gas-metal mix. The mixed material grows in volume as the product of interfacial surface area S and the diffusion layer thickness Δx_D, or $V_{\mathrm{mix}} = S \Delta x_D$. The hydro stirred volume is fully atomically mixed when $V_{\mathrm{mix}} \to V_{\mathrm{stir}}$. Subsequent increase of mix comes entirely from growth of the stirred volume, which does not depend on diffusion. Reference [3] has this limit as always satisfied for high Reynolds number flows provided turbulence is fully developed. It is an open question, however, whether ICF capsule implosions are of sufficient duration or steadiness to allow turbulence to fully develop and to grow the interfacial area to the size required in Ref. [3].

The diffusion-independent picture of mix may be correct, but it is not a conclusion that can be drawn from the behavior of passive scalar mixing into a neutral fluid shear layer. The transient ICF plasma implosion is a far more complex situation. The interface of interest is between two very different materials undergoing a rapid compression and heating causing changes in state that are extreme. Where the neutral fluid transport coefficient for viscosity, thermal conduction, diffusion, and the like are essentially constants, the plasma coefficients are highly variable. One example is the temperature scaling of $\sim T^{5/2}$. A plasma implosion tracked from 30 to 10 keV undergoes increases in viscosity thermal conduction, etc. by a factor of 10^6.

The first step in developing a sound physics base for the mix layer dynamics is to understand plasma diffusion. It is the purpose of this Letter to work out the basic structure of this layer as it develops from an initially sharp interface—a problem that has not previously been studied. We focus on heavy metal pushers as used in the double shell capsule designs [4–6].

The form of the equations of dissipative hydrodynamics for plasmas has long been studied [7–10], and partial results have been obtained for many of the transport coefficients. The mass diffusion subproblem has been examined recently [11–15]. The work in Ref. [15] focuses exclusively on the binary plasma mixture considered in this Letter and provides the complete hydrodynamic equations

with analytic formulas for all the transport coefficients. Diffusion is relative to the mass average fluid velocity. The interface layer can be considered to be imbedded in hydro flows of longer scale that produce the stirring. The full light ion (gas) mass flux is, from Ref. [15],

$$m_i\Gamma_i = -y_I n_i m_i D_{iI}\left[\alpha_{11}\left(\nabla \ln x_i + \frac{(x_i - y_i)}{n_i T_i}\nabla P_i + \frac{(z_i - y_i)}{n_i T_i}\nabla P_e + \frac{Z_{\text{eff}} - 1}{Z_{\text{eff}}}\frac{\alpha_T}{T_i}\nabla T_e\right) + \frac{3}{2}\alpha_{12}\nabla \ln T_i\right], \tag{1}$$

where the variables x_j, y_j, and z_j denote atom, mass, and charge fractions, respectively, with subscripts $j = i$ for the gas and $j = I$ for the metal. The thermal force transport coefficient α_T is a function of Z_{eff} and the coefficients α_{11} and α_{12} are functions of the ion coupling parameter $\Delta_I \equiv (m_i Z_I^2/m_I)(1 - y_i)/y_i$. In the isothermal limit examined in this Letter, only the concentration gradient and barodiffusion fluxes [16,17] are needed. There is general agreement on the form of these fluxes in Refs. [7–15], although only Ref. [15] contains the explicit analytic formulas used here. The other references would require working out some additional details. Preliminary work based on Ref. [11] has in fact reproduced the structure derived here with some differences in detail [18].

We consider the temperatures constant and equal for electrons and ions. The total pressure can then be written $P = P_i + P_e = (n + n_e)T = (\rho/m_i)[2y_i + (m_i/m_I)(Z_I + 1)(1 - y_i)]T$. Constant total pressure results when the density varies with the concentration according to

$$\rho = \frac{\rho_0}{[2y_i + (m_i/m_I)(Z_I + 1)(1 - y_i)]}, \tag{2}$$

with $\rho_0 = P/2T$ a constant. As the diffusion mixing layer evolves in time and the spatial profile $y_i(x)$ broadens, the mass spatial profile $\rho(x)$ must also move in accordance with Eq. (2). This requires nonzero pressure forces, since diffusion cannot cause net mass flow. Diffusion can, however, produce pressure imbalances, which then induce mass flow [19]. Our isobaric model of the diffusion layer assumes that the pressure will transiently depart from its constant value and relax the mass profile according to Eq. (2). This occurs on the fast, Euler, time scale so that in analyzing the slower diffusion process one can work with the relaxed, isobaric state. The light ion diffusion mass flux can now be simplified to

$$m_i\Gamma_i = -y_I n_i m_i D_{iI}\left[\alpha_{11}(\Delta_I)\left(\nabla \ln x_i + \frac{(z_i - x_i)}{n_i T_i}\nabla P_e\right)\right]. \tag{3}$$

The gas partial mass density ρ_i is chosen as the single mixture variable, dimensionless with the definition $a \equiv \rho_i/\rho_0$, so that pure gas is $a = 0.5$. The continuity equation $\partial\rho_i/\partial t + \nabla \cdot m_i\Gamma_i = 0$ can be reworked with substantial "mixture algebra" to give the nonlinear diffusion equation for the mixing layer,

$$\frac{\partial a}{\partial t} = \frac{\partial}{\partial x} D_0[d_c(a) + d_P(a)]\frac{\partial a}{\partial x}, \tag{4}$$

where the diffusion coefficient D_0, which does not depend on the mixture variable a, is given by

$$D_0 = 278\frac{4}{\ln\Lambda}\frac{A_i^{1/2}T^{5/2}}{\rho_0}\frac{Z_I + 1}{Z_I^2}\ \text{cm}^2/\text{sec}, \tag{5}$$

for T in keV and ρ_0 in g/cc. The dimensionless order unity functions that contain the nonlinear mixture dependences are for concentration gradient diffusion,

$$d_c(a) = \frac{\alpha_{11}(\Delta_I)}{\{1 - a[2 - (m_i/m_I)(Z_I + 1)]\}[a(Z_I - 1) + 1]}, \tag{6}$$

and for barodiffusion,

$$d_P(a) = d_c(a)\frac{a(1 - 2a)(Z_I - 1)^2}{[Z_I - a(Z_I - 1)]}. \tag{7}$$

The ionic coupling parameter Δ_I can be expressed in terms of a as $\Delta_I = Z_I^2(1 - 2a)/[a(Z_I + 1)]$.

We make the simplification of treating the Coulomb log as constant. The theory allows $\ln\Lambda$ to vary between collision pairs, $\ln\Lambda \to \ln\Lambda_{ij}$, and as a function of macroscopic parameters. The effects of strong coupling and related processes that modify $\ln\Lambda$ could be treated by exploiting this freedom. Preliminary work [18] indicates observable effects on the layer structure.

The solution of Eq. (4) gives the evolution of the diffusion layer between gas and metal. Its distinctive nonlinear structure depends on the functional dependence of the diffusion coefficient $d(a) = [d_c(a) + d_P(a)]$ on gas density as plotted in Fig. 1, where $m_i = 2$, $m_I = 197$, $Z_I = 77$, and $\alpha_{11}(Z) = (3\pi/32)(288 + 604\sqrt{2}Z + 217Z^2/4(72 + 61\sqrt{2}Z + 16Z^2))$, with $Z = \Delta_I$.

Note that the barodiffusion component dominates over most of the layer, but the profile asymmetry comes from the concentration gradient term. The transition from mixture to pure metal occurs on the left-hand side of the layer where $a \to 0$ and the diffusion coefficient $d_c(0) \to 1$. The barodiffusion component goes to zero at both edges of the layer. The transition to pure gas occurs at the right-hand edge where $a \to 1/2$ and the coefficient d_c is very small, $d_c \to 1.18(m_I/m_i)/(Z_I + 1)^2$. This is a characteristic of highly ionized heavy elements. It will give rise to a

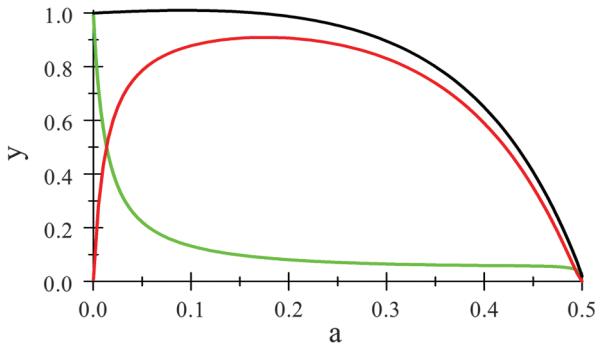

FIG. 1 (color). Diffusion coefficients for $m_I/m_i = 197/2$ and $Z_I = 77$; d_c, green curve; d_P, red curve; total, black curve.

diffusion "front" structure to the mixing-wave evolution with a sharp transition from mixing layer to pure gas that is in some respects analogous to the Marshak thermal wave [20] whose behavior is familiar from radiation hohlraum design.

Solutions to Eq. (4) can be found using the similarity variable,

$$\xi = \frac{x}{\sqrt{2\int_0^t dt' D_0(t')}}, \tag{8}$$

which transform Eq. (4) to

$$-\xi\frac{\partial a}{\partial \xi} = \frac{\partial}{\partial \xi}[d_c(a) + d_P(a)]\frac{\partial a}{\partial \xi}. \tag{9}$$

Note that the similarity transformation is exact analytically, and valid for $t > 0$. It also allows for the treatment of systems with time-varying temperature, density, and ionization state when they are spatially homogeneous over the layer width. We will fix these quantities and the diffusion coefficient D_0 so that $\xi = x/\sqrt{2D_0 t}$. The profile in the similarity variable ξ can be determined by converting Eq. (9) into two first-order equations and numerically solving with the standard Runge-Kutta method (e.g., rk4 from Ref. [21]). However, the solution is found with a shooting method to solve the boundary value problem using an initial value solver. From $\xi = 0$, one can iterate on the values of a and $da/d\xi$ until the boundary conditions are satisfied: $a = 0$ at $\xi \to -\infty$ and $a = 1/2$ at $\xi \to +\infty$ or $\xi = \xi_f$. The location of the wave front ξ_f, when it exists, is not unique until the condition of conservation of mass for the gas diffused into the metal is applied. For an idealized diffusion coefficient that goes to zero exactly at the mix layer gas boundary, one can show analytically that the profile inside the layer is linear at the location of the front, $a = 1/2 - \xi_f(\xi_f - \xi)/d'$, where $d' \equiv (d/da)d(a = 1/2)$. The transition to pure metal produces an extended gas profile of trace amounts exponentially decaying into the metal in the manner of a linear diffusion process.

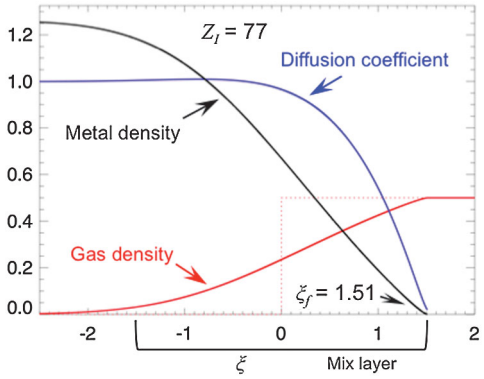

FIG. 2 (color). Similarity profiles for $m_I/m_i = 197/2$ and $Z_I = 77$.

The layer profiles are plotted in Fig. 2 as functions of the similarity variable ξ. It should be noted that although the diffusion coefficient does not go to zero (the blue line in Fig. 2), the metal still exhibits a well-defined front with clean gas to the right. Calculations for $Z_I = 10$ and $Z_I = 20$, where the diffusion coefficient was not small as $a \to 1/2$, did not result in a front. Metal profiles decayed exponentially into the gas extending to all distances.

Time-dependent numerical solutions were obtained to confirm the self-similar profile. The diffusion equation (4) is integrated in time with the profile-dependent coefficients in Eqs. (6) and (7) and with the coefficient D_0 set to one. Although nonlinear, the diffusion equation is not stiff and readily solved by conventional numerical methods. We confirmed the integration achieves the same results by explicit, implicit, or time-centered (Crank-Nicolson) differencing. Results at several times, $t = 0$, 20, 40, 60, and 80, are plotted in Fig. 3 using the self-similarity variable.

At the later times, the solutions clearly overlay and confirm the self-similarity. At early times, $t = 20$, it is evident that the nonlinear diffusion solution differs from the

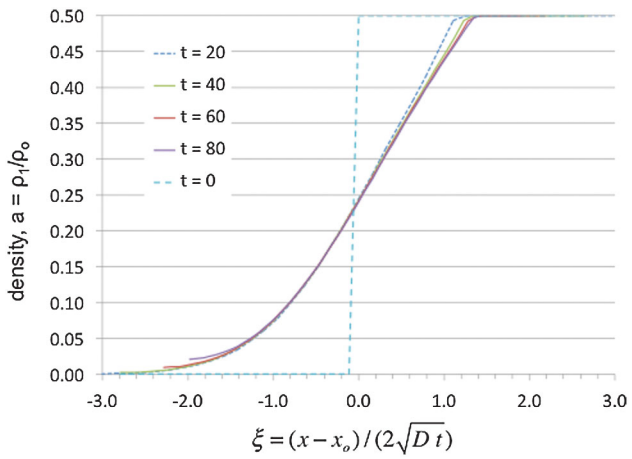

FIG. 3 (color). Time-dependent numerical solutions of a versus the similarity variable ξ for $m_I/m_i = 197/2$ and $Z_I = 79$.

self-similarity profile as it evolves from the discontinuous initial conditions. Self-similarity (to ~99%) is achieved in the numerical integration by time $t \sim 40$–50 corresponding to a scale length of 9–10. Higher grid resolution would reduce this time. Small differences, seen in the profiles as x approaches the left-hand boundary, result from the zero flux boundary conditions at a fixed spatial position starting to interfere with the spreading self-similar solution as time increases.

Simulations using the LSP code [22–24] were carried out to provide an independent validation of the theoretical results. LSP is a hybrid particle-in-cell simulation code, run here with a nonrelativistic inertial fluid electron component and two distinct kinetic particle ion species. Collisions between ions were handled via the binary collision model based on the method of Nambu and Yonemura [25] with a general Spitzer collision frequency. The initial conditions for the system included constant temperature ($T_e = T_{\rm D} = T_{\rm Al} = 4$ keV) for both ion species and the electrons. The interface between the ion species at time zero was a sharp discontinuity, with fully ionized aluminum at density of $\rho_I = 18.7$ g/cm^{-3} on the left and fully ionized deuterium at $\rho_i = 9.7$ g/cm^{-3} on the right of zero. The system was started in pressure equilibrium. Figure 4 displays the results of the simulation (dashed line) compared to the theoretical predictions given above at a time $t = 0.25$ nsec, when the layer width is ~2 μm, the deuteron Knudsen number is $N_{\rm Ki} \approx 10^{-3}$, and we expect valid hydrodynamics. The theoretical predictions, with no adjustable parameters, agreed in detail with the simulation results. Not only was the asymmetric self-similar density profile that was predicted above observed in the simulation, but the diffusion coefficient value of $D_0 = 7.2$ μm^2/nsec predicted by Eq. (5), using the same $\ln\Lambda = 3$ as LSP, agreed with the measured value found in the simulation by fitting the profiles to the similarity variable. The similarity constant from the theory for the Al-D interface, $\xi_f = 1.65$, coincided with the front location in the simulations.

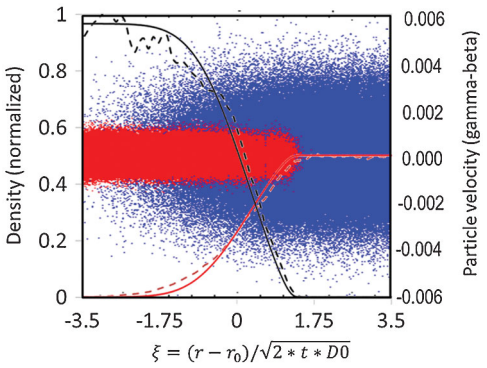

FIG. 4 (color). LSP simulation results (dashed line) compared to theory predictions (with no multipliers). Metal ions in red, gas ions in blue.

Of particular significance is verification of the assumption made in the theory of a fast relaxation of the pressure profiles to maintain the isobaric state (and the fast, by $\sim\sqrt{m_i/m_e}$, electron thermal conduction relaxation of the temperature profiles to maintain the isothermal state).

Practical implications and consequences for thermonuclear burn can be inferred from the integral characteristics of the layer. If the decaying gas profile tailing into the metal is ignored, the layer can be defined as centered on the initial interface, $\xi = 0$, and extending from $\xi = -\xi_f$ to $\xi = \xi_f$. Both gas and metal profiles are close to linear in this domain. The gas remains "clean" for $\xi > \xi_f$, which is significant for thermonuclear burn given the large effect on opacity of even trace metal amounts. The half-layer thickness and mass of gas within this layer are then

$$\Delta x_D = \xi_f \sqrt{2D_0 t}, \tag{10}$$

$$M_{gL} = S\rho_i \Delta x_D = S\rho_0 \xi_f \sqrt{D_0 t/2}, \tag{11}$$

where S is the interfacial surface area. Similarly, for the metal in the layer,

$$M_{mL} = \frac{S\rho_0 \xi_f}{(m_i/m_I)(Z_I + 1)} \sqrt{2D_0 t}, \tag{12}$$

and a metal-to-gas ratio of $M_{mL}/M_{gL} = 2m_I/m_i(Z_I + 1)$. This is the mass density ratio for the pure materials on either side of the interface ($M_{mL}/M_{gL} = 2.53$ for the deuterium-gold mixture we are using as an example with $\xi_f = 1.51$).

A measure of the importance of the diffusion mix layer for overall burn is the ratio of mix layer gas mass M_{gL} to the total gas mass in the ideal spherical volume, $M_g = 4\pi\rho_i R^3/3$. The mix layer gas is highly interdiffused with metal and has much lower burn performance. We write the interfacial area as $S = f_S 4\pi R^2$ to exhibit the factor f_S by which the initially spherical surface is increased due to asymmetric hydrodynamic flow. The mass ratio is then

$$\frac{M_{gL}}{M_g} = \frac{3S\Delta x_D}{4\pi R^3} = f_S \frac{3\Delta x_D}{R}. \tag{13}$$

Note that for a symmetric implosion with $f_S = 1$, the ratio M_{gL}/M_g exceeds 50% when the diffusion layer grows to 20% of the cavity radius. To be more quantitative, we take the burn time to be $t_B \sim R/c_s$, with $c_s = 4.0 \times 10^7 (T/A_i)^{1/2}$, and get, for an equimolar DT fuel mix,

$$\frac{M_{gL}}{M_g} = 0.0027 f_S \frac{T}{(2\rho_i R)^{1/2}}. \tag{14}$$

For perfectly spherical fuel volumes with a robust $\rho R \sim 1$ g/cm^2, the effect of diffusive mix will be small unless temperatures approach $T \sim 100$ keV. At lower

temperatures of order 10 keV, a modest amount of hydrodynamic stirring that increases the gas-metal interfacial area by the factor $f_S \sim 10$ would produce a significant effect from mix. Plasma diffusion can generate substantial levels of metal mixed into fuel with much less aspheric hydrodynamic activity than previously thought.

In a rapidly imploding ICF capsule, where plasma diffusion may increase 10^6-fold in a nanosecond, a very different and complementary physical picture of mix suggests itself. Hydrodynamic stirring originates from drive asymmetries and surface instabilities that are delayed in development and localized in scale. Turbulence is not fully developed. The gas-metal interfacial area increases, but much slower than in Ref. [3]. The diffusive spreading and area growth of the interface are separate processes whose product is the mix volume as in Eq. (13). Some fraction of the stirred volume is not mixed, $V_{\rm mix} < V_{\rm stir}$. In fact, diffusion layer formation may be negligible, $V_{\rm mix} \ll V_{\rm stir}$, until after ignition. Diffusion layer evolution would then proceed from an initial rapid formation $\Delta_D \propto t^{1/2}$ to a low velocity growth $d\Delta_D/dt \propto t^{-1/2}$ thereafter (behavior familiar from the Marshak thermal waves of a hohlraum). Such a picture, if substantiated, would make possible fully resolved simulations that used complete multispecies plasma transport equations.

This work was performed under the auspices of the Thermonuclear Burn Initiative at Los Alamos National Laboratory, LLC for the U.S. Department of Energy under Contract No. DE-AC52-06NA25396 and at Lawrence Livermore National Laboratory, LLC under Office of Science Contract No. DE-AC52-07NA27344.

[1] G. Dimonte and R. Tipton, Phys. Fluids **18**, 085101 (2006).
[2] D. Benard, F. Harlow, R. Rauenzahn, and C. Zemach, Los Alamos National Laboratoy Report No. LA-12303-MS, 1995.
[3] J. E. Broadwell and R. E. Briedenthal, J. Fluid Mech. **125**, 397 (1982).
[4] P. Amendt, J. D. Colvin, R. E. Tipton, D. E. Hinkel, M. J. Edwards, O. L. Landen, J. D. Ramshaw, L. J. Suter, W. S. Varnum, and R. G. Watt, Phys. Plasmas **9**, 2221 (2002).
[5] P. Amendt, Phys. Plasmas **13**, 042702 (2006).
[6] P. Amendt, J. Milovich, L. J. Perkins, and H. Robey, Nucl. Fusion **50**, 105006 (2010).
[7] J. M. Burgers, *Flow Equations for Composite Gases* (Academic, New York, 1969).
[8] S. I. Braginskii, *Reviews of Plasma Physics* (Consultants Bureau, New York, 1965), Vol. 1.
[9] R. B. Bird, W. E. Stewart, and W. E. Lightfoot, *Transport Phenomnon*, 2nd ed. (Wiley, New York, 2002).
[10] V. M. Zhdanov, *Transport Processes in Multicomponent Plasma* (CRC Press, New York, 2002).
[11] T. Haxhimali, R. E. Rudd, W. H. Cabot, and F. R. Graziani, Phys. Rev. E **90**, 023104 (2014).
[12] G. Kagan and X. Z. Tang, Phys. Plasmas **19**, 082709 (2012).
[13] G. Kagan and X. Z. Tang, Phys. Lett. A **378**, 1531 (2014).
[14] G. Kagan and X. Z. Tang, Phys. Plasmas **21**, 022708 (2014).
[15] K. Molvig, A. N. Simakov, and E. L. Vold, Phys. Plasmas **21**, 092709 (2014).
[16] P. Amendt, O. L. Landen, H. F. Robey, C. K. Li, and R. D. Petrasso, Phys. Rev. Lett. **105**, 115005 (2010).
[17] P. Amendt, S. C. Wilks, C. Bellei, C. K. Li, and R. D. Petrasso, Phys. Plasmas **18**, 056308 (2011).
[18] W. H. Cabot (private communication). Comparable similarity profiles produced from the transport formulation of Ref. [11].
[19] E. L. Vold, Los Alamos National Laboratoy Report No. LA-UR-13-27186, 2013.
[20] R. E. Marshak, Phys. Fluids **1**, 24 (1958).
[21] W. H. Press, S. A. Teukolsky, W. T. Vetterling, and B. P. Flannery, *Numerical Recipes in FORTRAN*, 2nd ed. (Cambridge University Press, Cambridge, England, 1992).
[22] T. P. Hughes, R. E. Clark, and S. S. Yu, Phys. Rev. ST Accel. Beams **2**, 110401 (1999).
[23] D. R. Welch, D. V. Rose, B. V. Oliver, and R. E. Clark, Nucl. Instrum. Methods Phys. Res., Sect. A **464**, 134 (2001).
[24] C. Thoma, D. R. Welch, R. E. Clark, N. Bruner, J. J. MacFarlane, and I. E. Golovkin, Phys. Plasmas **18**, 103507 (2011).
[25] K. Nanbu and S. Yonemura, J. Comput. Phys. **145**, 639 (1998).